Molecular Neurobiology (2022) 59:6141–6157
https://doi.org/10.1007/s12035-022-02965-6

# HDAC7 Activates IKK/NF-κB Signaling to Regulate Astrocyte-Mediated Inflammation

Jinwang Ye[1,2] · Suyue Zhong[1] · Yunsong Deng[1] · Xuanbao Yao[1] · Qiong Liu[1,3] · Jian-Zhi Wang[4] · Shifeng Xiao[1,3]

Received: 21 March 2022 / Accepted: 16 July 2022 / Published online: 25 July 2022


## Abstract

Class IIa histone deacetylases (HDAC) have been shown to drive innate immune cell-mediated inflammation in the peripheral system, but their roles in cerebral inflammatory responses remain largely unknown. Here, we elucidate that HDAC7 is selectively elevated in lipopolysaccharide (LPS)-challenged astrocytes both in vivo and in vitro. We identify that HDAC7 binds to the inhibitory kappa B kinase (IKK) to promote IKKα and IKKβ deacetylation and subsequent activation, leading to the activation of nuclear factor κB (NF-κB). Astrocyte-specific overexpression of HDAC7 results in NF-κB activation, pro-inflammatory gene upregulation and anxiety-like behaviors in mice, while downregulating HDAC7 reserves LPS-induced NF-κB activation and inflammatory responses. Furthermore, pharmacological inhibition of HDAC7 by a class IIa HDAC inhibitor attenuates LPS-induced NF-κB activation, inflammatory responses and anxiety-like behaviors both in vivo and in vitro. Together, our data reveal a novel mechanism of HDAC7 in astrocyte-mediated inflammation and suggest that targeting HDAC7 could be a potential therapeutic strategy for the treatment of anxiety and other inflammation-related diseases.

**Keywords** HDAC7 · IKK · NF-κB · Astrocyte · Inflammation · Anxiety

## Abbreviations

| | |
|---|---|
| LPS | Lipopolysaccharide |
| HDAC | Histone deacetylase |
| IKK | Inhibitory kappa B kinase |
| NF-κB | Nuclear factor κB |
| IκB | Inhibitor of κB |
| COX-2 | Cyclooxygenase-2 |
| iNOS | Inducible nitric oxide synthase |
| GFAP | Glial fibrillary acidic protein |
| C3 | Complement C3 |
| Lcn2 | Lipocalin-2 |
| Tnfα | Tumor necrosis factor α |
| OFT | Open field test |
| EPM | Elevated plus maze |

✉ Shifeng Xiao
sxiao@szu.edu.cn

Jinwang Ye
yejinwang1@foxmail.com

Suyue Zhong
doravzsy@163.com

Yunsong Deng
563011915@qq.com

Xuanbao Yao
453279504@qq.com

Qiong Liu
liuqiong@szu.edu.cn

Jian-Zhi Wang
wangjz@mail.hust.edu.cn

[1] Shenzhen Key Laboratory of Marine Biotechnology and Ecology, College of Life Sciences and Oceanography, Shenzhen University, Shenzhen 518060, Guangdong, China

[2] College of Physics and Optoelectronic Engineering, Shenzhen University, Shenzhen 518060, China

[3] Shenzhen Bay Laboratory, Shenzhen 518055, Guangdong, China

[4] Department of Pathophysiology, School of Basic Medicine, Key Laboratory of Education Ministry of China/Hubei Province for Neurological Disorders, Tongji Medical College, Huazhong University of Science and Technology, Wuhan 430030, China

## Introduction

Anxiety is a mental health disease characterized with excessive fear, anxiety, and avoidance of perceived threats in internal to oneself or the environment. Considering the ongoing COVID-19 pandemic that has resulted in quarantine and social isolation, the rise in individuals suffering from anxiety has been particularly noticeable. Accumulating evidence suggest a tight link between inflammation and the pathology in anxiety and other psychiatric disorders [1, 2]. Astrocytes are the most abundant glial cells and their dysfunction and activation have attracted increasing attention in the study of anxiety [3]. In the central amygdala, oxytocin-expressing astrocytes mediate neuronal activity and anxiolytic and positive reinforcement effects [4]. In the basolateral amygdala, lipopolysaccharide (LPS)-induced inflammation contributes to anxiety and depressive-like behavior [5]. Moreover, inhibition of astrocyte-mediated inflammation has been evidenced to show beneficial effects on anxiety-like disorders [6, 7]. However, the underlying mechanisms of astrocyte-mediated inflammation remain unclear.

The histone deacetylase (HDAC) family has been implicated in inflammatory process, and anti-inflammatory effects of HDAC inhibitors have been recognized [8]. However, clinical trials have raised the potential of undesirable effects occurring upon pan-HDAC inhibitor treatment [9, 10]. Thus, investigation of selective HDAC might bring new insights in improving the therapeutic efficacy. In particular, the class IIa HDACs (HDAC4, 5, 7, and 9) are distinct from other HDACs as they rarely associate with histone tails [11] and can shuttle between the cytoplasm and nucleus to regulate signaling transduction and gene expression [12]. In the peripheral immune system, class IIa HDACs are shown to modulate immune response and drive innate immune cell-mediated inflammation [13, 14]. For instances, in a macrophage-dependent autochthonous breast cancer mouse model, application of a selective class IIa HDAC inhibitor, TMP195, can induce the recruitment and differentiation of highly phagocytic and stimulatory macrophages within tumors [15]. Myeloid-specific overexpression of HDAC7 amplifies LPS-induced inflammatory signature, while pharmacological or genetic inhibition of HDAC7 attenuates LPS-inducible inflammatory responses [13]. Treatment of class IIa inhibitor confers beneficial effects in LPS-induced acute kidney injury mice model as well [16]. However, the function of class IIa HDACs in the cerebral inflammation has been largely unexplored.

Nuclear factor κB (NF-κB), a pro-inflammatory transcriptional factor, is a key regulator of inflammation in central nervous system [17]. Under physical conditions, NF-κB is sequestered in the cytoplasm by the inhibitor of κB (IκB). In the canonical NF-κB activation pathway, signal-induced IκB phosphorylation by inhibitor of κB kinase (IKK) promotes IκB ubiquitination and subsequent degradation, leading to the release and nuclear translocation of NF-κB [18, 19]. IKK is composed of three subunits including two homologous catalytic subunits IKKα and IKKβ and a regulatory subunit IKKγ [20]. Recent studies have established a close link between class IIa HDACs and IKK/NF-κB signaling. For instance, HDAC4-knockout macrophages display increased NF-κB activity and proinflammatory genes expression with enhanced NF-κB acetylation [21]. Moreover, HDAC4 can directly SUMOylate IκBα and prevent its polyubiquitination and degradation, resulting in the inhibition of NF-κB [22]. HDAC9 can binds to IKKα and IKKβ, causing their deacetylation and subsequent activation, which drive NF-κB activation in both macrophages and endothelial cells [23]. These studies revealed the critical and intricate role of class IIa HDACs in modulating NF-κB activity in different cells and tissue organ types. However, their involvements in the brain remain unclear.

Here, we exhibit that LPS stimulation specifically increases the mRNA and protein expression levels of HDAC7 in astrocytes both in vivo and in vitro, with other class IIa HDACs nearly unchanged. Astrocyte-specific overexpression of HDAC7 in hippocampal CA1 promotes NF-κB activation, astrocyte activation, and pro-inflammatory gene expression. Mechanically, HDAC7 binds to IKKα, IKKβ, and IKKγ, resulting in IKKα and IKKβ deacetylation and activation, which promotes NF-κB nuclear localization. Pharmacological inhibition or knockdown of HDAC7 rescues LPS-induced NF-κB activation, astrocyte-mediated inflammation and anxiety-like behaviors. Together, our results demonstrate a critical role of astrocytic HDAC7/IKK/NF-κB signaling in LPS-induced inflammatory responses and anxiety.

## Materials and Methods

### Animals, Stereotaxic Surgery, and Drug Treatment

Adult male C57BL/6 mice (2-month-old) were purchased from Changzhou Cavens Laboratory Animal Co., Ltd. The mice were housed in groups of four to five per cage with ad libitum access to food and water, and were maintained under a 12-h light/dark cycle (lights on at 7:00 p.m., off at 7:00 a.m.) at a stable temperature (22 ± 2 °C). In the present study, we have complied with all relevant ethical regulations for the animal testing and research. All procedures were approved by institutional guidelines and the Animal Care and Use Committee (Shenzhen University, Shenzhen,

China) of the university's animal core facility. Mice were anesthetized with isoflurane and placed on a stereotaxic apparatus, and then sterilized with iodophor and the scalp was incised along the midline of the head. Hole was stereotaxically drilled in the skull at posterior 2.1 mm, lateral 1.5 mm, and ventral 1.3 mm relative to the bregma. Using a microinjection system (World Precision Instruments), AAV-GfaABC1D-HDAC7-eGFP or control vector (1 μL, $5.0\times10^{12}$ viral genome per milliliter) was injected into bilateral hippocampal CA1 region at a rate of 0.125 μL/min, the needle was kept for 5 min before withdrawal, the skin was sutured and mice were placed beside on a heater for recovery. TMP195 was diluted to 7.5 mg/mL with sterile 0.9% saline containing 5% (vol/vol) Tween-80 and 20% (vol/vol) PEG-300.

## Behavioral Tests

### Open Field Test

The OFT is used to measure the anxiety-like behavior in mice. The OFT apparatus is made of transparent plastic (50 cm × 50 cm × 40 cm, length × width × height) and the central zone area was defined as 50% of the open field arena. Each mouse was brought to the room and acclimated for at least 1 h before the behavioral test. Individual mouse from each group was placed in the center area of the arena and permitted for free exploration. Their activity was videotaped from the top of the arenas for 10 min by a video camera. The time spent in the center area, the number of central area crossings, and center moving distance were recorded by video-tracking and behavioral analysis software (SMART v3.0 software).

### Elevated Plus Maze

Elevated plus maze (EPM) was performed to evaluate the anxiety-like behavior in mice. The EPM apparatus consists of two opposing open arms (66 cm × 6 cm) and two opposing closed arms (66 cm × 6 cm) intersecting at 90 degrees in the form of a plus, with a central area (6 cm × 6 cm). The EPM was elevated 50 cm above the floor in a dim and quiet room without any human disturbance during the test. Mouse from each group was placed in the center area and allowed to explore the EPM for 10 min freely. The time spent in open arms, the total number of entries into the open arm, and total distance in open arms were recorded by video-tracking and behavioral analysis software (SMART v3.0 software). Between each trial, the maze was cleaned with 75% ethanol.

## Cell Culture

For primary mouse astrocyte culture, astrocytes were isolated from 12 to 24 h neonatal C57BL/6 mice. The cortex was isolated and minced into ice-cold Hank's buffered saline solution, and incubated in 0.25% trypsin at 37 °C for 15 min. Then, the tissue was gently triturated eight to ten times to dissociate the cells and obtain a homogenous cell suspension. The density of cells was determined by a hemocytometer. Astrocytes were planted with the DMEM-high glucose medium containing 10% FBS onto poly-D-lysine-precoated flasks. After 5–7 days, when the cell density reached 75–90%, the astrocytes were sorted at shake cultivation rotating at 200–220 r/min overnight. Then, the medium was discarded, and the cells were incubated with DMEM containing 0.25% trypsin for 5 min, and centrifuged at 1000 g for 5 min after addition of the culture medium.

**Table 1** RT-qPCR primers used in the study

| Target gene | Forward | Reverse |
|---|---|---|
| HDAC4 | AGCAGCACCAGCAGTTCCT | CCGCTTCTTCCTCCTCACTCT |
| HDAC5 | AGCAGCACCAGCAGTTCCT | CACTCTCGCCATCCTCATCCT |
| HDAC7 | CGCAGCCAGTGTGAGTGTCT | GCTCGTTCCAGATGGTGTCAGTA |
| HDAC9 | GATGATGATGCCTGTGGTGGAT | TGCTGCTGCTGCTGAATAAGAA |
| Il-1α | CGCTTGAGTCGGCAAAGAAAT | CTTCCCGTTGCTTGACGTTG |
| Il-1β | GCAACTGTTCCTGAACTCAACT | ATCTTTTGGGGTCCGTCAACT |
| Il6 | TAGTCCTTCCTACCCCAATTTCC | TTGGTCCTTAGCCACTCCTTC |
| Tnfα | CCCTCACACTCAGATCATCTTCT | GCTACGACGTGGGCTACAG |
| C3 | AAG CAT CAA CAC ACC CAA CA | CTT GAG CTC CAT TCG TGA CA |
| Gfap | AGAAAGGTTGAATCGCTGGA | CGGCGATAGTCGTTA |
| Ptgs2 | GTCTGGTGCCTGGTCTGATGATG | TCTGATACTGGAACTGCTGGTTGAA |
| Nos2 | CCCTTCCGAAGTTTCTGGCAGCAGC | GGCTGTCAGAGCCTCGTGGCTTTGG |
| LCN2 | CAGGACTCAACTCAGAACT | GCTCATAGATGGTGCTGTA |
| β-actin | CCACCATGTACCCAGGCATT | CGGACTCATCGTACTCCTGC |

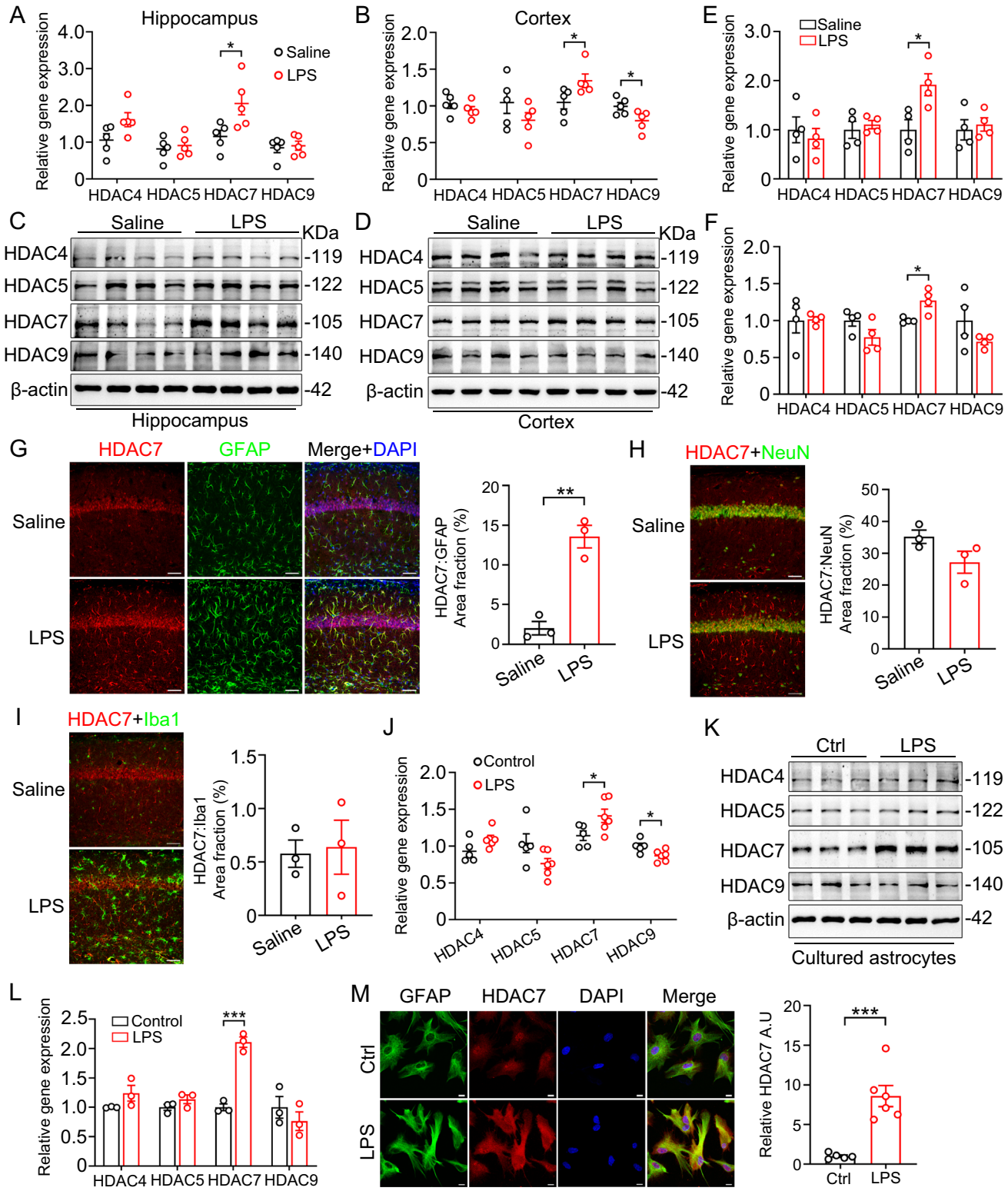
A
Hippocampus
Relative gene expression
Saline
LPS
HDAC4 HDAC5 HDAC7 HDAC9
B
Cortex
C
Saline
LPS
KDa
HDAC4
HDAC5
HDAC7
HDAC9
β-actin
-119
-122
-105
-140
-42
Hippocampus
D
Cortex
E
F
G
HDAC7
GFAP
Merge+DAPI
HDAC7:GFAP Area fraction (%)
H
HDAC7+NeuN
HDAC7:NeuN Area fraction (%)
I
HDAC7+Iba1
HDAC7:Iba1 Area fraction (%)
J
Control
K
Ctrl
Cultured astrocytes
L
M
GFAP
HDAC7
DAPI
Merge
Relative HDAC7 A.U

◂**Fig. 1** HDAC7 level is selectively increased in LPS-stimulated astrocytes in vivo and in vitro. mRNA expression of class IIa HDACs analyzed by RT-qPCR in hippocampus (**A**) and cortex (**B**) of LPS- and saline-injected mice (wildtype 2-mon-old C57BL/6 male were intraperitoneally injected with LPS (3 mg/kg) or normal saline and sacrificed 24 h after injection). $N=5$ mice for each group, unpaired Student's $t$ test. Representative western blots of HDAC4, HDAC5, HDAC7, HDAC9, and β-actin in hippocampal (**C**) and cortical (**E**) lysates of LPS-treated and control mice. Quantification of HDAC4, HDAC5, HDAC7, and HDAC9 protein levels in hippocampus (**D**) and cortex (**F**), β-actin was used as a loading control. $N=4$ mice for each group, unpaired Student's $t$ test. **G–I** Co-staining of GFAP, NeuN, Iba1, and HDAC7 in the hippocampus after LPS injection. Scale bars, 80 μm. **J** RT-qPCR analysis of HDAC4, HDAC5, HDAC7, and HDAC9 mRNA expression in primary cultured mouse astrocytes after stimulation with LPS (100 ng/ml) for 24 h. **K** Representative western blots of HDAC4, HDAC5, HDAC7, HDAC9, and β-actin in LPS-treated primary astrocytes. $N=3$ for each group, unpaired Student's $t$ test. **L** Quantification analysis of HDAC4, HDAC5, HDAC7, and HDAC9 protein levels normalized to β-actin. $N=3$ for each group, unpaired Student's $t$ test. **M** Representative immunofluorescence image of GFAP and HDAC7 co-staining in LPS-treated primary astrocytes. Data were expressed as mean ± SEM, $^{*}p<0.05$, $^{***}p<0.001$

After resuspension, cells were plated onto culture plate with $5\times10^5$ per well for western blotting and RT-qPCR analysis and $1\times10^5$ per well for cell imaging. The culture medium was changed every 3 days throughout the cultivation process.

HEK293 WT cells were cultured with 90% DMEM-high glucose medium and 10% fetal bovine serum (FBS), 100 U/ml penicillin, and 0.1 mg/ml streptomycin (all from Hyclone) at 37 °C in the presence of 5% $CO_2$. Transfection was performed with Neofect (Neofect biological Technology, Beijing) when cells were cultured to 70 ~ 80% confluence in six-well plates. 48 h after transfection, cells were collected and lysed for further research.

### *Western Blotting and Co-immunoprecipitation*

Mice hippocampal CA1 were carefully separated using a microtome in ice-cold PBS, then homogenized in RIPA buffer containing 1 mM PMSF and 0.1% cocktail. Cultured cells were washed with ice-cold PBS twice and homogenized in RIPA buffer as described. After centrifugation at 10,000 g for 15 min, the supernatant was extracted and protein concentration test was taken up, the loading buffer (50 Mm Tris–HCL, 2% SDS, 10% glycerol, pH 7.6) was added in the homogenates and samples were boiled at 95 °C for 10 min. The protein samples were separated by SDS/PAGE and transferred onto nitrocellulose membranes (Whatman), then incubated with primary antibodies at 4 °C overnight. Secondary antibody incubation was performed at room temperature for 1 h. Immunoreactive bands were visualized with an electroluminescence kit and scanned for densitometric analysis using an imaging system (Image Station 4000 M; Kodak).

For co-immunoprecipitation, cells after treatment were homogenized in RIPA buffer containing 1 mm PMSF and 0.1% cocktail, then centrifuged at 12,000 g for 10 min. The supernatant was incubated with primary antibodies at 4 °C for 6 h followed by a 2-h incubation with protein A + G agarose. The resins were washed three times with PBS, resuspended with 2 × loading buffer, and boiled at 95 °C for 10 min. Immuno-precipitates were analyzed by western blotting.

### RT-qPCR

Mice brain tissues were dissected and immediately frozen in liquid nitrogen. Cultured cells were quickly collected and incubated with ice-cold TRIzol (No. 15596026, Invitrogen, USA) after the medium removal. Total RNA isolation from mice brains and cultured cells were performed following the manufacturer's protocol. The RNA concentration and purity were measured using a NanoDrop 2000 spectrophotometer (Thermo Scientific, USA). The RNA-to-cDNA reverse transcription reaction was carried out using a Prime Script RT Kit (RR047A, Takara, Japan). Briefly, right before reverse transcription reaction, the genomic DNA removing reaction was performed at room temperature for 30 min, and then, the reaction mixture was added to the RNA solution, and the RNA/reagent mixture was incubated at 37 °C for 15 min, further heated at 85 °C for 5 s, and cooled to 4 °C. RT-qPCR was performed using SYBR Master Mix on a Bio-Rad Connect Real-Time PCR platform (Bio-Rad, USA). The reaction was carried out in a DNA thermal cycler under the following conditions: 95 °C for 30 s, 39 cycles of 95 °C for 5 s and 60 °C for 30 s, 72 °C for 30 s, and 95 °C for 15 s, 60 °C for 30 s, 95 °C for 5 s and 4 °C for 60 s. The resulting Cq values were calculated (using the $2^{-\Delta\Delta CT}$ method), and β-actin was used as a housekeeping gene. The RT-qPCR primer sequences are listed in Table 1.

### Immunofluorescence

Cultured cells were fixed in 4% (vol/vol) paraformaldehyde for 15 min and permeabilized in phosphate buffer containing 0.5% triton X-100. Non-specific binding was blocked by

PBST buffer containing 3% BSA for 1 h. Primary antibodies were incubated at 4 °C overnight. The secondary antibodies conjugated to Alexa-Fluor 488/546 were added to the coverslip for 1 h at 37 °C, followed by Hoechst staining for 10 min. The coverslips were washed and mounted onto slides. All the images were observed with the LSM880 confocal microscope (Zeiss, Germany).

### Viruses, Reagents, and Antibodies

The IKKα-HA, IKKβ-HA, IKKγ-HA, IκBα-HA, and EGFP-HDAC7 plasmids were constructed in the pcDNA3.1 vector. The HDAC7 overexpression lentivirus lenti-GfaABC1D-HDAC7-P2A-eGFP, HDAC7 knockdown lentivirus lenti-GfaABC1D-shHDAC7-eGFP(mir30), AAV-GfaABC1D-HDAC7-eGFP, and corresponding controls were constructed and packaged by Obio Technology (Shanghai, China), and the target sequences of HDAC7 are TGCGCTACAAAC CCAAGAAAT and CCATGTTTCTGCCAAATGTTT. Lentiviruses were used in primary astrocytes with Multiplicity of infection (MOI) of 10. AAV2/8 was used in mice experiments.

Lipopolysaccharide (LPS) from Escherichia coli, strain 055: B5 was purchased from Absin (Shanghai, China). TMP195 (a selective class IIa HDAC inhibitor) was purchased from Selleck (Shanghai, China). All other reagents were from Sigma-Aldrich (USA).

IKKα (1:500 for WB, 2682), IKKβ (1:500 for WB, 2678), IKKγ (1:500 for WB, 2695), IκBα (1:500 for WB, 4814), Iba1 (1:50 for IF, 36,618), NF-κB (1:500 for WB, 1:100 for IF, 1:100 for IP, 8242), p-NF-κB-Ser468 (1:500 for WB, 3039), p-NF-κB-Ser536 (1:500 for WB, 3033), HA Tag (1:500 for WB, 1:100 for IP, 3724), acetylated-lysine (1:1000 for WB, 9441), IgG (1:100 for IP, 2729), GFAP (1:1000 for WB, 1:200 for IF, 36,707), iNOS (1:500 for WB, 1:100 for IF, 13,120), Il1α (1:500 for WB, 50,794), P38 (1:1000 for WB, 8690), p-P38 (1:1000 for WB, 4511), ERK1/2 (1:1000 for WB, 4695), p- IKKα/β (1:500 for WB, 2697), and p-ERK1/2 (1:500 for WB, 4370) were from Cell Signaling. HDAC4 (1:1000 for WB, 07–1490), and HDAC7 (1:1000 for WB, 1:100 for IF, 1:100 for IP, H2662) were from Thermo Scientific. HDAC5 (1:1000 for WB, ab55403), HDAC9 (1:1000 for WB, ab109446), NeuN (1:200 for IF, ab104224), LaminB1 (1:1000 for WB, ab16048), COX-2 (1:500 for WB, ab179800), Iba1 (1:100 for IF, ab5076), and beta-actin (1:1000 for WB, ab6272) were from Abcam. Iba1 (1:200 for IF, 012–26,723) was from Wako.

### Statistical Analysis

Data are expressed as mean ± SEM and analyzed using the GraphPad Prism 8 statistical software. The one-way or two-way ANOVA was used to determine the differences among four groups, and the Student's *t* test was used for two groups. The significance was assessed at $p < 0.05$.

**Fig. 2** Astrocyte-specific overexpression of HDAC7 leads to inflammation and anxiety-like behaviors in mice. AAV-GfaABC1D-HDAC7-eGFP or the empty vector was stereotaxically infused into the hippocampal CA1 subset of 2-month-old wildtype mice. After expression for 1-month, behavioral tests were performed. **A** Representative confocal image showing the co-expression of GFP, HDAC7, and GFAP in the dorsal hippocampal CA1 subset of 2-month-old mice. Scale bar, 50 μm. Quantification shows the relative GFAP expression level in GFP positive cells. $N = 6$ mice for each group, unpaired Student's *t* test. **B** Astrocytic overexpression of HDAC7 increases mRNA levels of Il-1α, Il-1β, Il6, Tnfα, Gfap, and C3 analyzed by RT-qPCR in the hippocampus. $N = 6$ mice for each group, unpaired Student's *t* test. **C**–**K** Astrocytic overexpression of HDAC7 activates NF-κB activity. **C** Representative western blots of HDAC7, GFAP, p-IKKα/β(S176/180), IKKα, IKKβ, p-NF-κB(S468), p-NF-κB(S536), NF-κB, and β-actin in the HDAC7-overexpressing and control hippocampal CA1 lysates. Quantification analysis of HDAC7 protein levels normalized to β-actin (**D**), GFAP protein levels normalized to β-actin (**E**), IKKα protein levels normalized to β-actin (**F**), IKKβ protein levels normalized to β-actin (**G**), p-IKKα/β(S176/180) normalized to IKKα (**H**), p-IKKα/β(S176/180) normalized to IKKβ (**I**), p-NF-κB(S468) normalized to total NF-κB (**J**), and p-NF-κB(S536) normalized to total NF-κB (**K**). $N = 5$ mice for each group, unpaired Student's t test. **L** Representative immunofluorescence image showing enhanced nuclear NF-κB expression in HDAC7-overexpressing and control astrocytes. Scale bar, 10 μm. **M** Quantification of nuclear NF-κB fraction in GFP positive cells. $N = 21$–24 cells from 3 mice for each group, unpaired Student's *t* test. **N**–**R** Overexpression of HDAC7 results in anxiety-like behaviors in the open field test. In this paradigm, the exploring performance in the center region (green frame area) is tested (**N**, left half panel). HDAC7-overexpressing mice show decreased center moving distance (**O**), center exploring time (**P**), and center entries (**Q**) in the open field test. The total moving distance remain unchanged (**R**). $N = 8$–11 mice, unpaired Student's *t* test. **N** and **S**–**U** Overexpression of HDAC7 results in anxiety-like behaviors in the elevated plus maze. In this paradigm, the exploring performance in the open arm (green frame area) is tested (**N**, right half panel). HDAC7 mice show decreased open arm travel distance (**S**), open arm exploring time (**T**), and open arm entries (**U**) in the elevated plus maze. $N = 8$–11 mice, unpaired Student's *t* test. Data were expressed as mean ± SEM, $^{*}p < 0.05$, $^{**}p < 0.01$, $^{***}p < 0.001$

## Results

### *HDAC7 Levels Are Increased in LPS-Stimulated Astrocytes* In Vivo *and* In Vitro

Class IIa HDAC drives innate immune response in the peripheral immune system. To explore the involvement of IIa HDACs in the inflammation in the brain, 2-month-old male C57BL/6 mice were intraperitoneally injected with LPS (3 mg/kg) or normal saline and sacrificed 24 h after injection. Interestingly, through RT-qPCR tests, we found that LPS-treatment dramatically increased HDAC7 mRNA levels

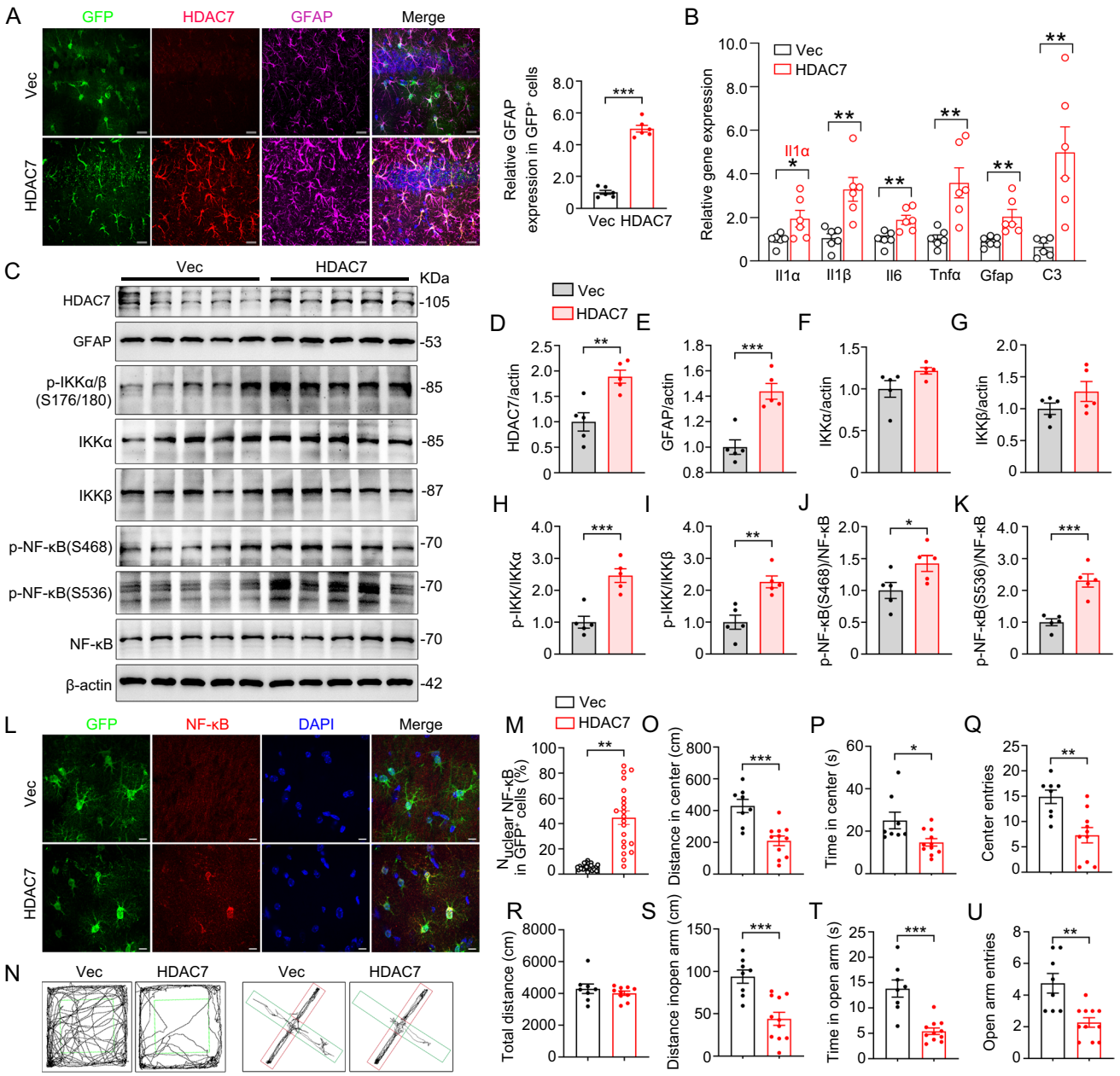


both in the hippocampus and cortex (Fig. 1A and B), with a slightly reduction of HDAC9 in the cortex and other HDACs unchanged (Fig. 1B). Further studies confirmed uniquely upregulated HDAC7 protein levels in both the hippocampus (Fig. 1C and E) and cortex (Fig. 1D and F) as well. Strikingly, co-immunostaining showed that elevated HDAC7 was mostly located in astrocytes in LPS-injected mouse brain (Fig. 1G), while neuronal HDAC7 remained unaffected (Fig. 1H). HDAC7 expression in microglia was relatively low and little difference was seen after LPS treatment (Fig. 1I). To further identify the role of IIa HDACs in astrocytes, primary cultured astrocytes were treated with LPS (100 ng/ml) for 24 h. Consistent with the results observed in vivo, LPS-treatment markedly increased HDAC7 mRNA level (Fig. 1J) and protein expression (Fig. 1K and L) in cultured astrocytes. LPS-induced HDAC7 upregulation was detected mainly in the cytoplasm as shown by immunofluorescence staining (Fig. 1M). These in vivo and in vitro data suggest that HDAC7 may play a unique role in LPS-induced astrocyte activation and related inflammation.

## Astrocyte-Specific Overexpression of HDAC7 Leads to Inflammation and Anxiety-Like Behaviors in Mice

To verify the role of HDAC7 in astrocyte-mediated inflammation in vivo, we specially overexpressed HDAC7 in

astrocytes by stereotaxically injecting AAV-GfaABC1D-HDAC7-eGFP or AAV-GfaABC1D-eGFP into the dorsal hippocampal CA1 subset of 2-month-old wildtype male C57BL/6 mice. The expression of AAV-GfaABC1D-HDAC7-eGFP in astrocytes was confirmed by immunofluorescence imaging at one month after injection (Fig. 2A). The HDAC7 protein level increased on average to ~ 1.9-fold of the control in the HDAC7-overexpressing brains (Fig. 2C and D). Overexpression of HDAC7 induces distinct astrocyte activation, as shown by hypertrophic morphology and enhanced glial fibrillary acidic protein (GFAP) expression (Fig. 2 , C, and E). Interestingly, significant microglia activation was found in AAV-GfaABC1D-HDAC7-eGFP positive areas as well (supplementary Fig. 1). RT-qPCR analysis of Il-1α, Il-1β, Il6, tumor necrosis factor α (Tnfα), Gfap, and complement C3 (C3) revealed remarkable pro-inflammatory responses in HDAC7-overexpressing mice (Fig. 2B). In light of the central role of NF-κB in astrocyte-mediated inflammation and the resemblance of HDAC7-related inflammatory gene expression with NF-κB-driven transcriptional responses, we hypothesized that NF-κB might be a downstream effector of HDAC7. As suggested, western blotting analysis showed that astrocytic overexpression of HDAC7 increased p-IKKα/β levels at Ser176 or Ser180 normalized to total IKKα or IKKβ (Fig. 2C, H, and I) and enhanced NF-κB phosphorylation levels at Ser468 and Ser536 normalized to total NF-κB (Fig. 2C, J, and K). The protein levels of IKKα and IKKβ remain unchanged between HDAC7-overexpression and control GFP mice (Fig. 2C, F, and G). Immunofluorescence staining also identified enhanced nuclear localization of NF-κB in HDAC7-overexpressing astrocytes compared to GFP-expressing astrocytes (Fig. 2L and M). These data implicate that NF-κB could act as a downstream effector of HDAC7.

Given the prominent inflammatory response in HDAC7-overexpressing mice, the effects of HDAC7 on psychiatric and cognitive behaviors were measured. We observed obvious anxiety-like behaviors in HDAC7-overexpressing mice, evidenced by reduced center distance (Fig. 2O), center exploring time (Fig. 2P), and center entries (Fig. 2Q) in the open field test (OFT) and decreased travel distance (Fig. 2S), spending time (Fig. 2T), and entries (Fig. 2U) in the open arm in elevated plus maze (EPM) test. The total moving distances of the mice in OFT were not affected by HDAC7 overexpression (Fig. 2R). Interestingly, HDAC7-overexpressing mice performed normally as the controls in the Morris water maze (data not shown). Thus, we concluded that astrocytic overexpression of HDAC7 promotes astrocyte-driven inflammatory responses and anxiety-like behaviors involving NF-κB signaling.

## HDAC7 Activates IKK Through Binding to and Deacetylating IKKα and IKKβ.

To gain mechanistic insights in HDAC7 and NF-κB activation, coimmunoprecipitation experiments were carried out by co-transfection of HDAC7 and IKKα, IKKβ, IKKγ or IκBα respectively in HEK293 cells. HDAC7 was shown to bind to IKKα, IKKβ and IKKγ, but not IκBα (Fig. 3A, D, G, and J). Of note, we observed increased protein levels of HA-tagged IKKα, IKKβ, and IκBα with reduced HA-tagged IKKγ level (Fig. 3A, B, D, E, G, H, J, and K). To explore the underlying consequence of HDAC7-IKK interactions, we determined the acetylation status of IKKα, IKKβ, and IKKγ. The acetylation of IKKα and IKKβ were reduced in HDAC7-overexpressing cells (Fig. 3A, C, D, and F), while IKKγ acetylation level kept unvaried (Fig. 3G and I). IKK deacetylation is believed to enhance their activity. Thus, we tested IKKβ activity and found increased IKKβ activity as evidenced by increased phosphorylation levels of NF-κB P65 at Ser468 and Ser536 in an immunoprecipitation-based kinase activity assay (Fig. 3L, M, O). To further extend our findings in astrocytes, we overexpressed HDAC7 in primary cultured mouse astrocytes via infection of lenti-GfaABC1D-HDAC7-GFP or lenti-GfaABC1D-GFP. We found increased nuclear NF-κB level and unaffected cytoplasm NF-κB level upon HDAC7 overexpression (Fig. 3P and Q). In contrast, little effect of HDAC7 on p38 mitogen-activated protein kinase (MAPK) and extracellular signal-regulated protein kinases 1/2 (ERK1/2) signaling was detected (Supplementary Fig. 2), further corroborating the specificity of the downstream signaling events induced by HDAC7/IKK interactions. Together, these findings identified IKK/NF-κB signaling as a key downstream effector linking HDAC7 to astrocyte-driven inflammatory responses.

## Inhibition of HDAC7 Attenuates LPS-Induced NF-κB Activation and Inflammatory Responses in Cultured Astrocytes

To identify whether knockdown of HDAC7 can rescue NF-κB activation and inflammation responses in astrocytes, we downregulated HDAC7 in cultured mouse astrocytes through infection of lenti-GfaABC1D-shHDAC7-eGFP-WPRE (miR30) or control lenti-GfaABC1D-eGFP-WPRE (miR30) for 5 days, and then treated cells with LPS (100 ng/ml) for 24 h. We found that knockdown of HDAC7 efficiently inhibited LPS-induced NF-κB phosphorylation at Ser468 and Ser536 (Fig. 4A, B, C). Moreover, IKKα and IKKβ phosphorylation at Ser176/180 were also limited by HDAC7 knockdown (Fig. 4D, E, F). The total protein levels of IKKα and IKKβ were comparable in GFP control and HDAC7 knockdown cells (supplementary Fig. 3),

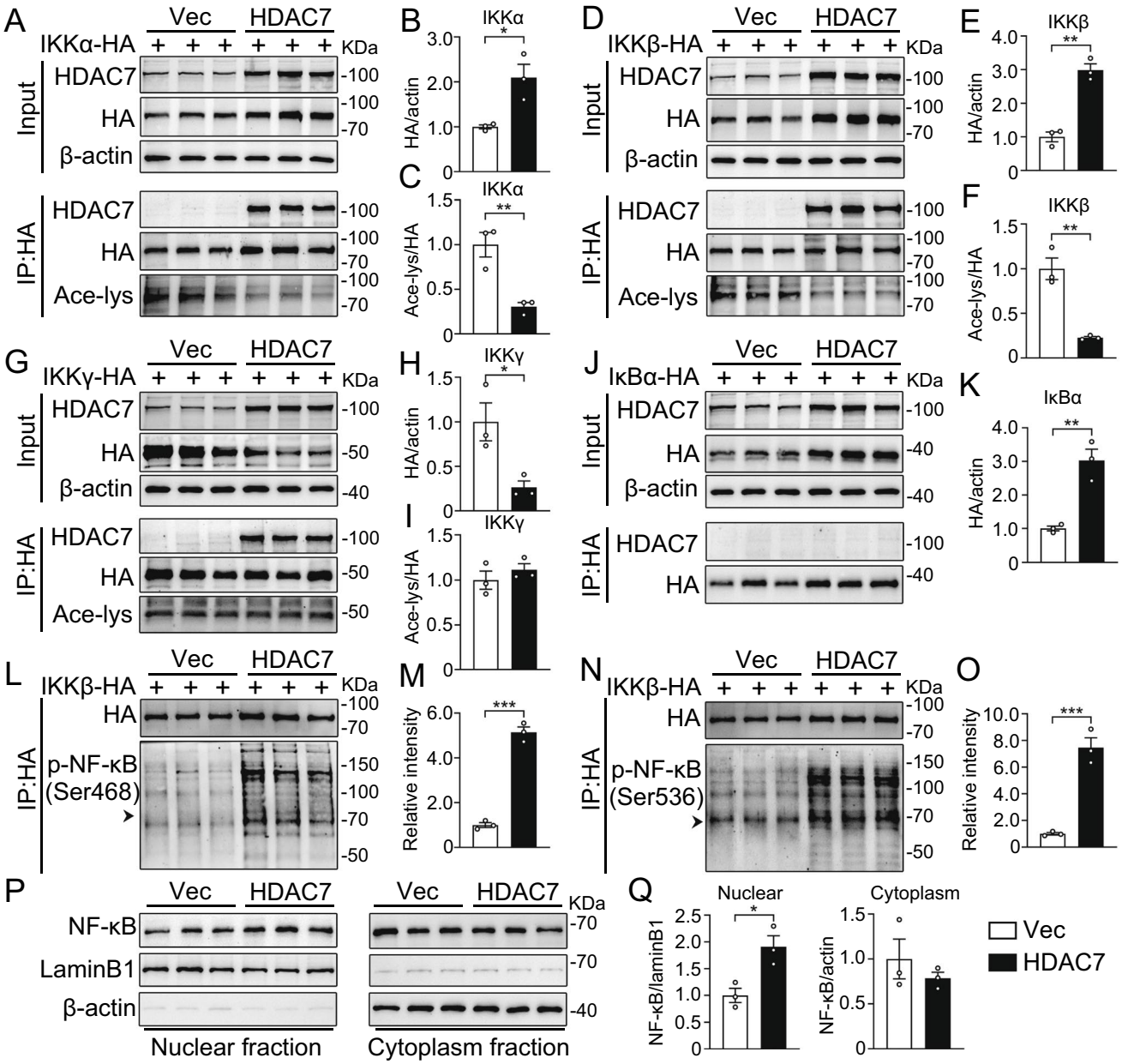


**Fig. 3** HDAC7 activates IKK through binding to and deacetylating IKKα and IKKβ. HEK293 cells were transiently co-transfected with pcDNA3.1-HDAC7 and individual components of the IKK complex (HA-IKKα, HA-IKKβ, or HA-IKKγ) or HA-IκBα. Co-immunoprecipitation with anti-HA antibodies was performed after transfection for 24 h. **A**–**F** HDAC7 binds to and deacetylates IKKα and IKKβ. Representative immunoblots of HDAC7, HA, and Ace-lysine in HA-immunoprecipitated components and input fraction of IKKα + HDAC7 group (**A**) and IKKβ + HDAC7 group (**D**) are shown respectively. Quantification of total IKKα normalized to β-actin (**B**) and acetylated IKKα normalized to total IKKα (**C**). Quantification of total IKKβ normalized to β-actin (**E**) and acetylated IKKβ normalized to total IKKβ (**F**). $N = 3$ for each group, unpaired Student's $t$ test. **G**–**I** HDAC7 binds to IKKγ with no effects on IKKγ acetylation. **G** Representative immunoblots show expression level of HDAC7, HA, and Ace-lysine in HA-immunoprecipitated components and input fraction of IKKγ + HDAC7 and IKKγ + Vec cells. Quantification of total IKKγ normalized to β-actin (**H**) and acetylated IKKγ normalized to total IKKγ (**I**). $N = 3$ for each group, unpaired Student's $t$ test. **J**–**K** HDAC7 has no interaction with IκBα. **J** Representative immunoblots show expression level of HDAC7, HA in HA-immunoprecipitated components and input fraction of IκBα + HDAC7 and control cells. **K** Quantification of total IκBα normalized to β-actin. $N = 3$ for each group, unpaired Student's $t$ test. **L**–**O** HDAC7 improves IKK activity showed by increased levels of p-NF-κB(S468) (**L**) and p-NF-κB(S536) (**N**) in HA-immunoprecipitated fraction. **M** Quantification analysis of p-NF-κB(S468) normalized to total IKKβ. **O** Quantification analysis of p-NF-κB(S536) normalized to total IKKβ. $N = 3$ for each group, unpaired Student's $t$ test. **P** and **Q** Overexpression of HDAC7 increases NF-κB nuclear localization. **P** Representative immunoblots of NF-κB, LaminB1 and β-actin in nuclear and cytoplasm fraction. **Q** Quantification of nuclear NF-κB normalized to LaminB1 and cytoplasm NF-κB normalized to β-actin. $N = 3$ for each group, unpaired Student's $t$ test. Data were expressed as mean ± SEM, $^{*}p < 0.05$, $^{**}p < 0.01$, $^{***}p < 0.001$

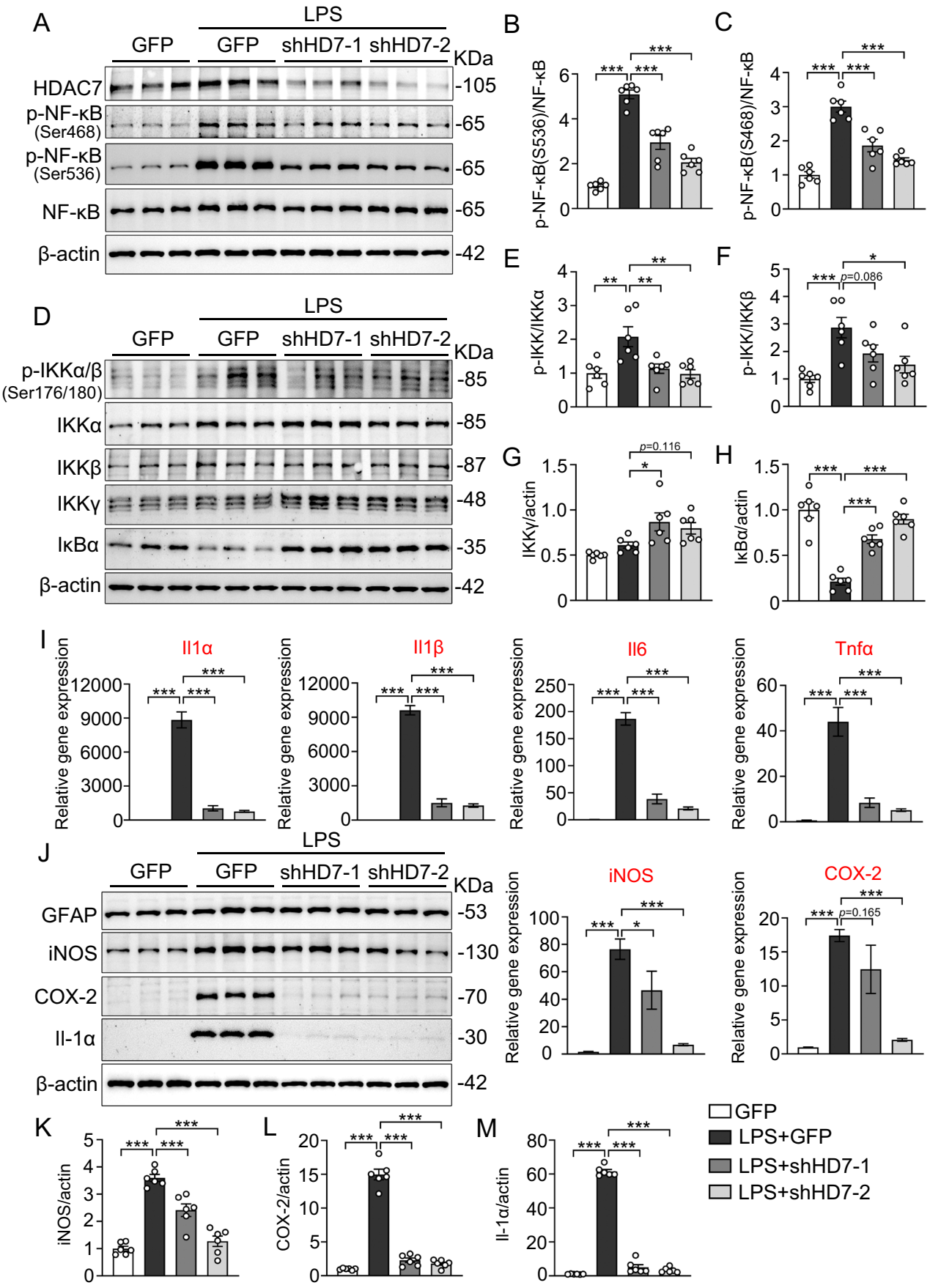
A
LPS
GFP
GFP
shHD7-1
shHD7-2
KDa
HDAC7
-105
p-NF-κB (Ser468)
-65
p-NF-κB (Ser536)
-65
NF-κB
-65
β-actin
-42
B
p-NF-κB(S536)/NF-κB
C
p-NF-κB(S468)/NF-κB
D
p-IKKα/β (Ser176/180)
-85
IKKα
-85
IKKβ
-87
IKKγ
-48
IκBα
-35
β-actin
-42
E
p-IKK/IKKα
F
p-IKK/IKKβ
p=0.086
G
IKKγ/actin
p=0.116
H
IκBα/actin
I
Il1α
Il1β
Il6
Tnfα
Relative gene expression
J
GFAP
-53
iNOS
-130
COX-2
-70
Il-1α
-30
β-actin
-42
iNOS
COX-2
p=0.165
K
iNOS/actin
L
COX-2/actin
M
Il-1α/actin
GFP
LPS+GFP
LPS+shHD7-1
LPS+shHD7-2

◂**Fig. 4** Genetic knockdown of HDAC7 suppresses LPS-induced NF-κB activation and inflammatory responses in primary cultured astrocytes. **A**–**C** Knockdown of HDAC7 inhibits LPS-induced NF-κB activation in cultured astrocytes. **A** Representative western blots showing protein levels of HDAC7, p-NF-κB(S468), p-NF-κB(S536), NF-κB, and β-actin in control and LPS-treated primary cultured mouse astrocytes (astrocytes were infected with Lenti-GfaABC1D-HDAC7-T2A-GFP or Lenti-GfaABC1D-T2A-GFP for 5 days, and then treated with LPS (100 ng/ml) for 24 h). **B** Quantification analysis of p-NF-κB(S468) normalized to total NF-κB. **C** Quantification analysis of p-NF-κB(S536) normalized to total NF-κB. $N=6$ for each group, one-way ANOVA, Dunnett's post hoc analysis. **D**–**H** Knockdown of HDAC7 suppresses IκBα degradation with little effects on IKK expression. **D** Representative western blots showing protein levels of p-IKKα/β(S176/180), IKKα, IKKβ, IKKγ, IκBα, and β-actin in control and LPS-stimulated primary mouse astrocytes as described above. Quantification of p-IKKα/β(S176/180) normalized to IKKα (**E**), p-IKKα/β(S176/180) normalized to IKKβ (**F**), IKKγ normalized to β-actin (**G**), and IκBα normalized to β-actin (**H**). $N=6$ for each group, one-way ANOVA, Dunnett's post hoc analysis. **I**–**M** Knockdown of HDAC7 inhibits LPS-induced inflammatory responses in cultured astrocytes. **I** RT-qPCR analysis of Il-1α, Il-1β, Il6, Tnfα, iNOS, and COX-2 in control and LPS-stimulated primary cultured mouse astrocytes as described above. **J** Representative western blots showing protein levels of GFAP, iNOS, COX-2, Il-1α, and β-actin in control and LPS-treated primary cultured mouse astrocytes. Quantification of iNOS (**K**), COX-2 (**L**), and Il-1α (**M**) normalized to β-actin. $N=6$ for each group, one-way ANOVA, Dunnett's post hoc analysis. Data were expressed as mean ± SEM, $^{*}p<0.05$, $^{**}p<0.01$, $^{***}p<0.001$

while IKKγ was slightly increased by downregulating HDAC7 (Fig. 4D and G). In addition, HDAC7 knockdown cells showed augmented IκBα protein level compared to GFP cells in LPS-treated group (Fig. 4D and H). We also found that HDAC7 knockdown attenuated LPS-induced pro-inflammatory gene expression, as shown by markedly reduced mRNA levels of Il-1α, Il-1β, Il6, Tnfα, cyclooxygenase-2 (COX-2), and inducible nitric oxide synthase (iNOS) (Fig. 4I). Furthermore, LPS-induced protein expressions of COX-2, iNOS, and Il-1α were also abolished in HDAC7 knockdown cells (Fig. 4J, K, L, M).

Previous studies have reported that TMP195, a selective class IIa HDAC inhibitor with high affinity of HDAC7, may have potential in attenuating inflammatory response [16, 23]. Thus, we studied the effect of TMP195 in the mouse primary astrocytes by pretreating the cells with TMP195 (3/5 μM) for 1 h, and then with the mixture of LPS (100 ng/ml) and TMP195 (3/5 μM) for 24 h. Consistent with the results of genetically HDAC7 knockdown, TMP195 treatment dose-dependently blocked LPS-induced NF-κB phosphorylation at Ser468 and Ser536 (Fig. 5A, B, C), and attenuated the LPS-induced NF-κB nuclear translocation (Fig. 5D and E). Correspondingly, the reduced mRNA levels of NF-κB-targeted pro-inflammatory molecules Il-1α, Il-1β, Il6, Tnfα, COX-2, and iNOS were confirmed in TMP195-treated cells by RT-qPCR analysis (Fig. 5F). Further western blotting analysis of iNOS, COX-2 and Il-1α also verified the anti-inflammatory effects of TMP195 (Fig. 5G, H, I, J). Collectively, these results identified HDAC7 as a pivotal driver of IKK/NF-κB pathway in LPS-induced astrocyte-mediated inflammation.

### *Pharmacological HDAC7 Inhibition Attenuates Inflammation, Gliosis, and Anxiety-Like Behaviors* In Vivo

Given the anti-inflammatory effects of TMP195 in vitro, we examined the therapeutic implication of TMP195 in vivo. 2-month-old male C57BL/6 mice were intraperitoneally pre-injected with TMP195 (30/50 mg/kg) 2 h before injection of LPS or control saline (3 mg/kg, intraperitoneal injection), and followed by a second injection of TMP195 (30/50 mg/kg, intraperitoneal injection) 6 h after LPS treatment (Fig. 6A). Consistent with the in vitro findings, western blotting showed that TMP195 treatment ameliorated LPS-induced NF-κB phosphorylation at Ser468 and Ser536 in the hippocampus (Fig. 6B, C, D) and cortex (Fig. 6F, G, H), along with decreased GFAP expression (Fig. 6E and I). RT-qPCR analysis of Il-1α, Il-1β, Tnfα, Gfap, C3, and lipocalin-2 (Lcn2) also revealed a comprehensively reduced inflammatory response in TMP195-treated mouse hippocampus (Fig. 6J) and cortex (Fig. 6K). Simultaneously, LPS-induced astrocytes and microglia activation in the hippocampus were also attenuated as demonstrated by mitigated GFAP and Iba1 expression and preserved resting morphology (Fig. 7A, B, C). Specially, LPS-induced nuclear NF-κB activation in astrocytes was also attenuated upon TMP195 treatment (Fig. 7D and E). Together, these results suggest that pharmacological inhibition with TMP195 attenuates LPS-induced NF-κB activation and inflammatory responses in vivo.

Given that astrocytic overexpression of HDAC7 induces anxiety-like behaviors, we thus evaluated the therapeutic effects of TMP195 treatment on anxiety via the open field test and elevated plus maze test (Fig. 7F). In the OFT, treatment with high concentration (50 mg/kg) of TMP195 arrested LPS-induced behavioral disorders, as shown by restored moving distance (Fig. 7G) and exploring time (Fig. 7H) in the center region, while low concentration (30 mg/kg) of TMP195 exhibited no significant therapeutic effects. The total moving distances of the mice in the OFT test were comparable in all four groups (Fig. 7I). In the elevated plus maze test, both low and high concentrations (30/50 mg/kg) of TMP195 treatment efficiently rescued LPS-induced anxiety-like behaviors (Fig. 7J), as demonstrated by increased travel distance (Fig. 7K), spending time (Fig. 7L), and entries (Fig. 7M) in the open arm. Notably, the rescue effect of TMP195 exhibited a dose-dependent manifestation. Collectively, these results demonstrate that therapeutic HDAC7 inhibition with TMP195 prevents LPS-induced inflammation, gliosis and anxiety-like behaviors.

## Discussion

In the present study, we demonstrate that astroglial HDAC7 is a key regulator of LPS-induced astrocyte-mediated inflammatory responses and anxiety-like behaviors. Among the four IIa HDACs, HDAC7 is selectively elevated in LPS-challenged astrocytes both in vivo and in vitro. We have shown that HDAC7 directly deacetylates IKKα and IKKβ to enhance IKK activity, resulting in NF-κB activation, inflammatory gene expression and anxiety. Moreover, genetic or pharmacological inhibition of HDAC7 can effectively prevent LPS-induced NF-κB activation, astrocyte-driven inflammatory responses and anxiety-like behaviors both in vivo and in vitro, supporting

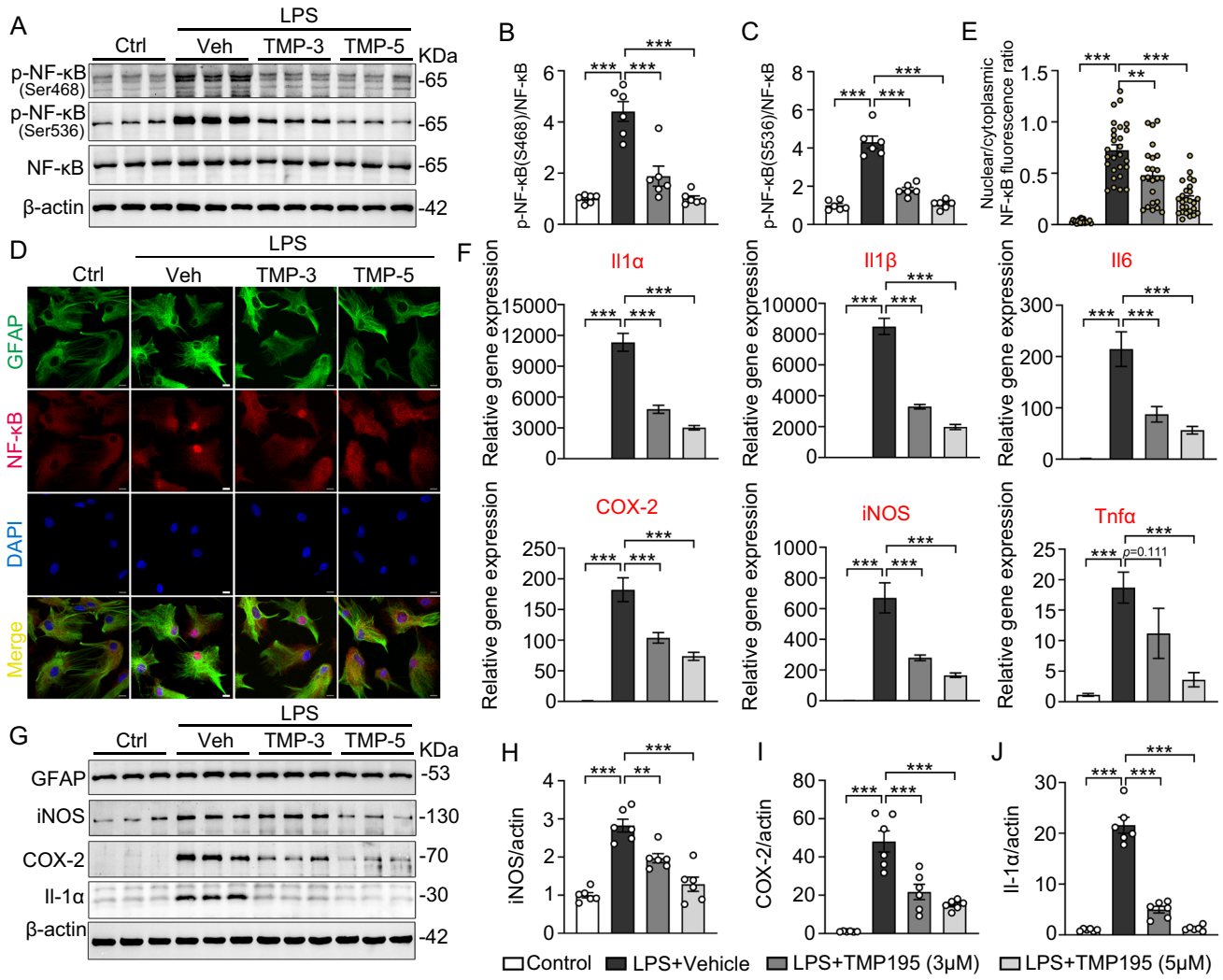


**Fig. 5** Pharmacological inhibition of HDAC7 with TMP195 suppresses LPS-induced NF-κB activation and inflammatory responses in primary cultured astrocytes. **A**–**C** TMP195 blocks LPS-induced NF-κB phosphorylation in cultured astrocytes. **A** Representative western blots showing protein levels of p-NF-κB(S468), p-NF-κB(S536), NF-κB, and β-actin in LPS- and TMP195-treated primary cultured mouse astrocytes (astrocytes were incubated with LPS (100 ng/ml), LPS (100 ng/ml) + TMP195 (3 μM), LPS (100 ng/ml) + TMP195 (5 μM), or control vehicle for 24 h). **B** Quantification of p-NF-κB(S468) normalized to total NF-κB. **C** Quantification of p-NF-κB(S536) normalized to total NF-κB. $N = 6$ for each group, one-way ANOVA, Dunnett's post hoc analysis. **D** Representative confocal images showing decreased nuclear NF-κB expression by TMP195 in LPS-stimulated astrocytes described as above. Scale bar, 10 μm. **E** Quantification of nuclear/cytoplasm NF-κB fluorescence ratio. $N = 21$–$37$ cells from 6 independent dishes for each group, one-way ANOVA, Dunnett's post hoc analysis. **F**–**J** TMP195 reverses LPS-induced inflammatory responses in cultured astrocytes. **F** RT-qPCR analysis of Il-1α, Il-1β, Il6, Tnfα, iNOS, and COX-2 in LPS and TMP195- treated astrocytes described as above astrocytes described as above. **G** Representative western blots showing protein levels of GFAP, iNOS, COX-2, Il-1α, and β-actin in primary astrocytes treated as described above. Quantification of iNOS (**H**), COX-2 (**I**), and Il-1α (**J**) normalized to β-actin. $N = 6$ for each group, one-way ANOVA, Dunnett's post hoc analysis. Data were expressed as mean ± SEM, $^{**}p < 0.01$, $^{***}p < 0.001$

a potential anti-inflammatory therapeutic strategy of targeting HDAC7.

Glia cell activation and inflammation are the leading cause of LPS-induce anxiety-like behaviors in mice. Our data showed that pharmacological inhibition of HDAC7 with TMP195 rescued LPS-induced anxiety-like behaviors, as demonstrated by restored distance, time, and entries in the center zone in the open field test and increased mobility to exploring the open arm in the elevated plus maze test in TMP195-treated mice compared to vehicle-treated mice. These beneficial effects could be attributed to TMP195-attenuated inflammatory responses, as shown by reduced mRNA levels of Il-1α, Il-1β, Tnfα, Gfap, C3, and Lcn2. This is in accordance with previous studies that described the beneficial effects on anxiety-like behaviors by blocking inflammation [1, 7]. In addition, inflammatory response is a common hallmark pathology of multiple neurodegenerative diseases, such as Alzheimer's disease and Parkinson disease; our positive data on LPS-challenged models might bring new insights in these chronic inflammatory diseases.

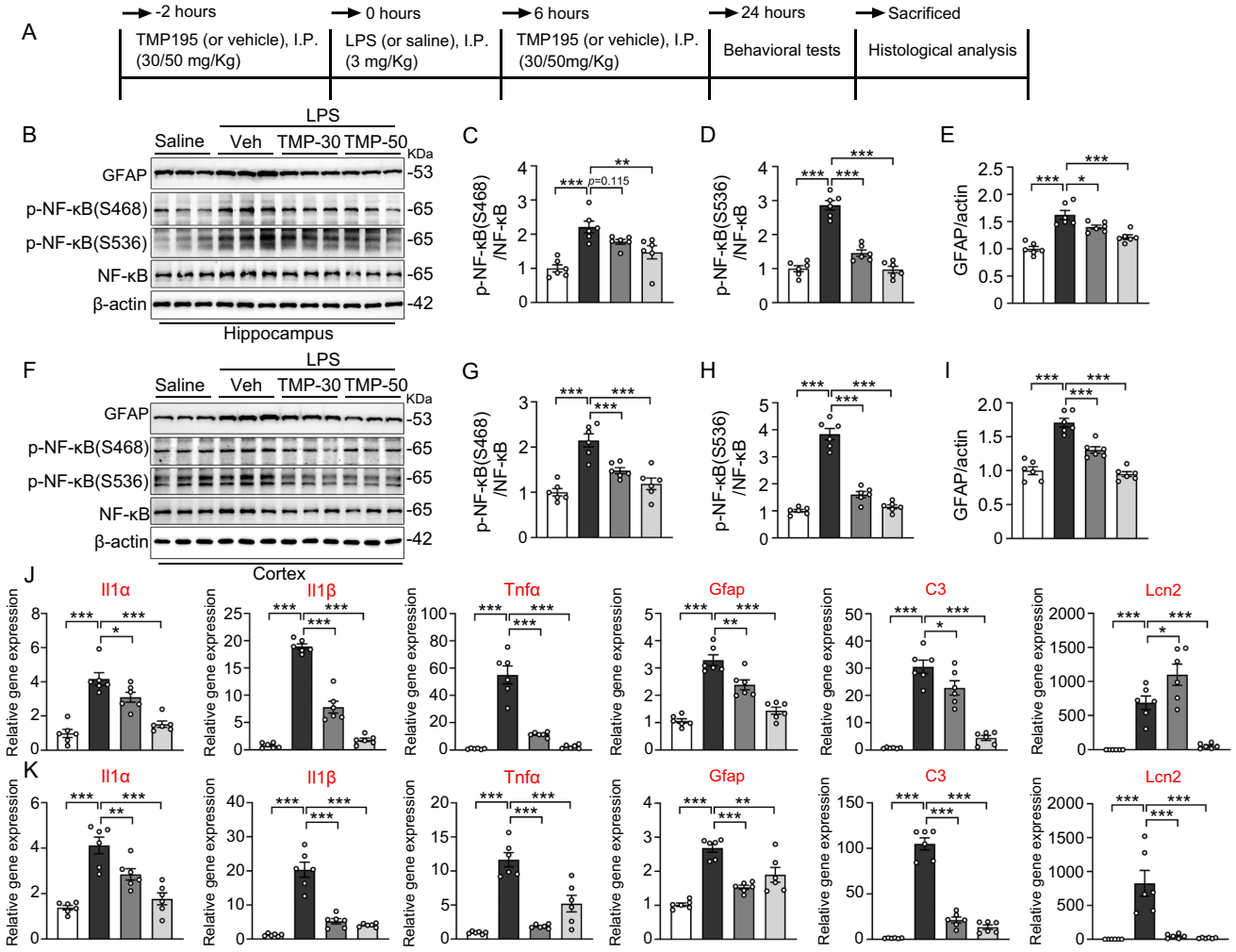


**Fig. 6** TMP195 decreases LPS-induced NF-κB activation and inflammation in vivo. **A** Schematic diagram of the experimental procedure in mice. 2-month-old wildtype C57BL/6 male mice were pre-injected with TMP195 (30/50 mg/kg) or vehicle 2 h before LPS (3 mg/kg) injection and received another injection of TMP195 (30/50 mg/kg) 6 h after LPS treatment. **B–I** TMP195 attenuates LPS-induced NF-κB activation in vivo. **B** Representative western blots showing protein levels of GFAP, p-NF-κB(S468), p-NF-κB(S536), NF-κB, and β-actin in hippocampus. **C–E** Quantification of p-NF-κB(S468) normalized to total NF-κB (**C**), p-NF-κB(S536) normalized to total NF-κB (**D**), and GFAP normalized to β-actin (**E**) in hippocampus. **F** Representative western blots showing protein levels of GFAP, p-NF-κB(S468), p-NF-κB(S536), NF-κB, and β-actin in cortex. **G–I** Quantification of p-NF-κB(S468) normalized to total NF-κB (**G**), p-NF-κB(S536) normalized to total NF-κB (**H**), and GFAP normalized to β-actin (**I**) in cortex. $N=6$ for each group, one-way ANOVA, Dunnett's post hoc analysis. **J** and **K** TMP195 reverses LPS-induced inflammatory gene expression in vivo. **J** RT-qPCR analysis of Il-1α, Il-1β, Tnfα, Gfap, C3, and Lcn2 gene expression in hippocampus. **K** RT-qPCR analysis of Il-1α, Il-1β, Tnfα, Gfap, C3, and Lcn2 gene expression in cortex. $N=6$ for each group, one-way ANOVA, Dunnett's post hoc analysis. Data were expressed as mean ± SEM, $^{*}p<0.05$, $^{**}p<0.01$, $^{***}p<0.001$

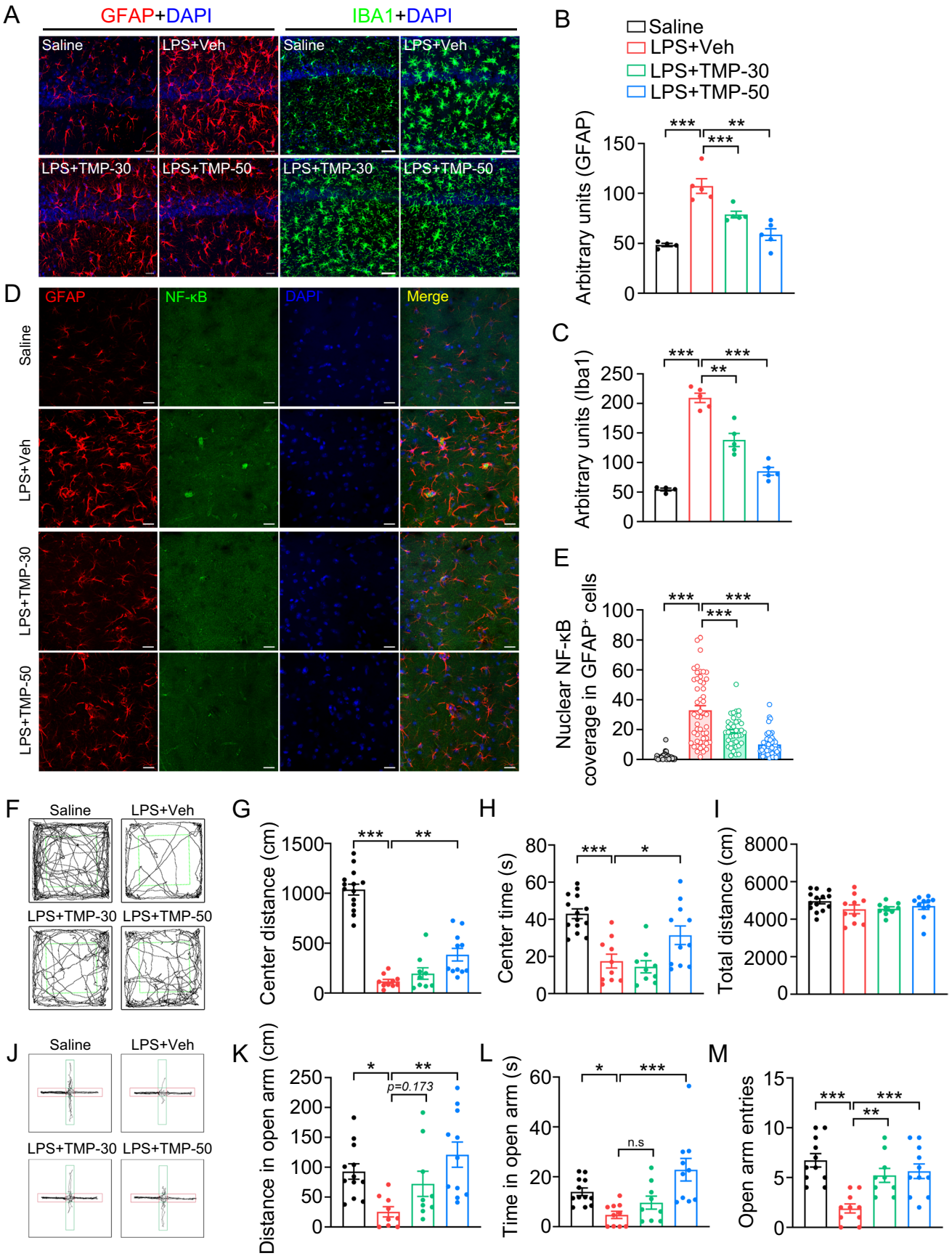
A
GFAP+DAPI
IBA1+DAPI
Saline
LPS+Veh
LPS+TMP-30
LPS+TMP-50
B
Saline
LPS+Veh
LPS+TMP-30
LPS+TMP-50
Arbitrary units (GFAP)
C
Arbitrary units (Iba1)
D
GFAP
NF-κB
DAPI
Merge
E
Nuclear NF-κB coverage in GFAP⁺ cells
F
G
Center distance (cm)
H
Center time (s)
I
Total distance (cm)
J
K
Distance in open arm (cm)
p=0.173
L
Time in open arm (s)
n.s
M
Open arm entries

◂**Fig. 7** TMP195 reverses LPS-induced gliosis and anxiety-like behaviors in vivo. **A–C** TMP195 limits LPS-induced gliosis. **A** Representative confocal image of GFAP and Iba1 in the hippocampal CA1 subset. Scale bar, 40 μm. **B** Quantification of GFAP and **C** Iba1 immunofluorescence intensity in the hippocampus. $N = 4–5$ for each group, one-way ANOVA, Dunnett's post hoc analysis. **D** and **E** TMP195 attenuates LPS-induced nuclear NF-κB activation in the astrocytes. **D** Representative hippocampal confocal images showing decreased nuclear NF-κB expression by TMP195 in LPS-injected mice. Scale bar, 40 μm. **E** Quantification of nuclear NF-κB fluorescence coverage in GFAP positive cells. $N = 38–54$ cells from 4–5 mice for each group, one-way ANOVA, Dunnett's post hoc analysis. **F–I** TMP195 attenuates LPS-induced anxiety-like behaviors in the open field test. In this test, the exploring performance in the center region (green frame area) is tested. **F** Representative moving traces of mice during the open field test. TMP195 treatment attenuates LPS-induced exploring disorders represented by increased center moving distance (**G**) and center exploring time (**H**) in the open field test. **I** The total moving distances are comparable in all four groups. $N = 9–14$ mice, one-way ANOVA, Dunnett's post hoc analysis. **J–M** TMP195 ameliorates LPS-induced anxiety-like behaviors in the elevated plus maze. **J** Representative moving traces of mice during the elevated plus maze. TMP195 treatment improved exploring capacity of LPS-injected mice shown by increased open arm travel distance (**K**), open arm exploring time (**L**), and open arm entries (**M**) in the elevated plus maze. $N = 9–12$ mice, one-way ANOVA, Dunnett's post hoc analysis. Data were expressed as mean ± SEM, $^{*}p < 0.05$, $^{**}p < 0.01$, $^{***}p < 0.001$

HDAC inhibition was described as potent anti-inflammatory strategy in several immune-mediated diseases [8, 24]. In the present study, we focused on class IIa HDACs and found that HDAC7 level is selectively increased in astrocytes both in vivo and vitro upon LPS treatment. Further, in vivo studies on astrocytes through delivery of AAV-GfaABC1D-HDAC7-eGFP into the hippocampal CA1 subset demonstrate an apparent astrogliosis and increased pro-inflammatory responses in HDAC7-overexpressing brain. Interestingly, similar increases in HDAC7 expression in inflammatory macrophages and enhanced inflammatory signature in myeloid-specific HDAC7 overexpressing macrophages upon LPS stimulation have been reported by *Sweet*'s group [13, 14]. Despite the consistent aspects between our study and that of *Sweet*'s group, there were noticeable differences. Specially, *Sweet*'s group reported increased inflammatory gene expression in HDAC7-overexpressing macrophages dependent on Toll-like Receptor 4 activation through LPS stimulation [13], whereas we observed enhanced inflammatory responses and astrogliosis independent of stimulation of exogenous antigens. This may be explained by the cell-type/tissue-restricted discrepancies or by the mechanic differences mediated by HDAC7 in macrophages and astrocytes. Indeed, we demonstrate here that HDAC7 activates IKK/NF-KB signaling to regulate astrocytic inflammation, different from the HDAC7-PKM2 signaling axis described by *Sweet*'s group.

NF-κB has been identified as a key transcriptional activator of astrocytic activation and inflammatory responses [25, 26]. Upon extracellular stimuli, IKK could be activated promptly, resulting in IκB phosphorylation and subsequent degradation by the proteasome, eventually promoting NF-κB nuclear translocation and pro-inflammatory gene transcription [20]. IKK activity is controlled by multiple posttranslational modifications, including phosphorylation and acetylation. Although a body of literature was generated on phosphorylation-mediated IKK activation and deactivation, the molecular regulating machinery involved in acetylation and deacetylation such as HDACs remained to be elucidated. In the current study, we demonstrated that HDAC7 could deacetylate IKKα and IKKβ and thus strengthen IKK activity, evidenced by upregulated NF-κB phosphorylation and nuclear NF-κB level. Highly consistent with our results, a previous study reported that HDAC9, another member of class IIa HDACs, can activate IKK through deacetylation of IKKα and IKKβ and promote NF-κB signaling activation [23]. Moreover, upon LPS stimulation, we observed augmented IκBα expression in HDAC7-knockdown cells, which also suggest an impaired IκBα degradation and infer a reduced IKK activity by downregulating HDAC7. Anyway, a well-defined deacetylation site on IKKα and IKKβ mediated by HDAC7 remains unclear; more mass spectrometry analysis is needed in the future. The activating effects of HDACs in NF-κB signaling have also been reported in other HDAC families. For examples, NF-κB acetylation is increased in HDAC1/2 double knockout mice [27], HDAC3 directly interacts with NF-κB p65 and is involved in the removal of the inhibitory NF-κB p65 acetylation [28], and inhibition of HDAC6 suppresses LPS-activated NF-κB signaling pathway in RAW264.7 macrophages [29]. Our exploration on HDAC7 provides new mechanic insights for NF-κB signaling study.

Previous reports in peripheral immune systems have provided evidence for the anti-inflammatory effect of targeting class IIa HDACs [13, 23]. By using TMP195, a selective class IIa HDAC inhibitor, in LPS-induced inflammation models, we observed reduced inflammatory responses including Il1α, Il1β, Tnfα, and C3, attenuated gliosis and reversed anxiety-like behaviors, implying that HDAC7 is a critical regulator of LPS-induced astrocyte-driven inflammatory responses. However, the involvement of other HDACs in the TMP195-treated studies cannot be rudely ruled out. Indeed, we declared here that HDAC7 has a dominant role, but multiple other class IIa HDACs could interact with IKK and contribute to inflammatory responses. For example, HDAC5 interact with IKKβ [30] and HDAC9 interact with both IKKα and IKKβ in HEK293 cells [23]. In vivo studies also demonstrate that knockdown of HDAC5 reduces LPS-induced inflammatory gene expression [31] and knockout of HDAC9 reduces vascular inflammation in a mouse model

of atherosclerosis [23]. Thus, it is possible that HDAC5 and HDAC9 may be partly involved in therapeutic effects accompanied by TMP195. It is uncertain whether specific knockout of astrocytic HDAC7 in vivo has a protective function in astrocyte-based inflammation. The creation of mice with tissue-specific knockout of HDAC7 in astrocytes may address this issue. Of note, we also observed that TMP195 treatment reverses LPS-induced microglia activation. Microglia are resident immune cells in the brain and play a crucial role in inflammation involving microglia-astrocyte crosstalk. The endogenous crosstalk between astrocytes and microglia regulates anti-inflammatory actions via the C3/C3aR signaling pathway. Previous studies have demonstrated that complement C3 released by NF-κB-activated astrocytes can modulate microglia immune homeostasis through C3a receptor expressed on microglia [32, 33], and knockout of C3 reduces microglia activation and proinflammatory cytokines levels [34, 35]. Indeed, we observed reduced C3 expression in both hippocampus and cortex of TMP195-treated mice compared with the control LPS-treated mice, providing a potential explanation for the blocking effects of TMP195 on microglia immune response.

To conclude, this study demonstrated a mechanistic explanation for the prominence of astrocytic HDAC7 in LPS-induced NF-κB activation and astrocyte-mediated inflammation and provided a novel therapeutic strategy of targeting HDAC7 for preventing inflammation and anxiety.

**Supplementary Information** The online version contains supplementary material available at https://doi.org/10.1007/s12035-022-02965-6.

**Acknowledgements** The authors thank the Instrumental Analysis Center of Shenzhen University for technical assistance.

**Author Contribution** Conceptualization, J. Y. and S. X.; investigation, J. Y., S. Z., Y. D., and X. Y.; writing manuscript, J. Y. and S. X.; funding acquisition, J. Y. and S. X.; resources, S. X., Q. L., and J. W.; supervision, S. X. and Q. L.

**Funding** This work was financially supported by the Shenzhen Science and Technology Innovation Commission (JCYJ20180507182417779, JCYJ20200109110001818), the Natural Science Foundation of China (82101493), and the China Postdoctoral Science Foundation (2021M692191).

**Data Availability** The datasets used or analyzed during the current study are available from the corresponding author on reasonable request.

## Declarations

**Ethics Approval** All animal experiments were approved by institutional guidelines and the Animal Care and Use Committee (Shenzhen University, Shenzhen, China) of the university's animal core facility.

**Consent to Participate** Not applicable.

**Consent for Publication** Not applicable.

**Conflict of Interest** The authors declare no competing interests.

## References

1. Lama A et al (2022) Palmitoylethanolamide dampens neuroinflammation and anxiety-like behavior in obese mice. Brain Behav Immun 102:110–123
2. Fang Y et al (2022) Fluoxetine inhibited the activation of A1 reactive astrocyte in a mouse model of major depressive disorder through astrocytic 5-HT2BR/beta-arrestin2 pathway. J Neuroinflammation 19(1):23
3. Rossi S et al (2017) Neuroinflammation drives anxiety and depression in relapsing-remitting multiple sclerosis. Neurology 89(13):1338–1347
4. Wahis J et al (2021) Astrocytes mediate the effect of oxytocin in the central amygdala on neuronal activity and affective states in rodents. Nat Neurosci 24(4):529–541
5. Zheng ZH et al (2021) Neuroinflammation induces anxiety- and depressive-like behavior by modulating neuronal plasticity in the basolateral amygdala. Brain Behav Immun 91:505–518
6. Shim HS et al (2019) Role of astrocytic GABAergic system on inflammatory cytokine-induced anxiety-like behavior. Neuropharmacology 160:107776
7. Zhuang X et al (2022) IL-33 in the basolateral amygdala integrates neuroinflammation into anxiogenic circuits via modulating BDNF expression. Brain Behav Immun 102:98–109
8. Shakespear MR et al (2011) Histone deacetylases as regulators of inflammation and immunity. Trends Immunol 32(7):335–343
9. Giaccone G et al (2011) Phase II study of belinostat in patients with recurrent or refractory advanced thymic epithelial tumors. J Clin Oncol 29(15):2052–2059
10. Ljubenkov PA et al (2021) Effect of the histone deacetylase inhibitor FRM-0334 on progranulin levels in patients with progranulin gene haploinsufficiency: a randomized clinical trial. JAMA Netw Open 4(9):e2125584
11. Lahm A et al (2007) Unraveling the hidden catalytic activity of vertebrate class IIa histone deacetylases. Proc Natl Acad Sci U S A 104(44):17335–17340
12. Martin M, Kettmann R, Dequiedt F (2007) Class IIa histone deacetylases: regulating the regulators. Oncogene 26(37):5450–5467
13. Das Gupta K et al (2020) Class IIa histone deacetylases drive toll-like receptor-inducible glycolysis and macrophage inflammatory responses via pyruvate kinase M2. Cell Rep 30(8):2712-2728 e8
14. Shakespear MR et al (2013) Histone deacetylase 7 promotes Toll-like receptor 4-dependent proinflammatory gene expression in macrophages. J Biol Chem 288(35):25362–25374
15. Guerriero JL et al (2017) Class IIa HDAC inhibition reduces breast tumours and metastases through anti-tumour macrophages. Nature 543(7645):428–432
16. Zhang W et al (2020) Class IIa HDAC inhibitor TMP195 alleviates lipopolysaccharide-induced acute kidney injury. Am J Physiol Renal Physiol 319(6):F1015–F1026
17. Kopitar-Jerala N (2015) Innate immune response in brain, NF-kappa B signaling and cystatins. Front Mol Neurosci 8:73
18. Wertz IE, Dixit VM (2010) Signaling to NF-kappaB: regulation by ubiquitination. Cold Spring Harb Perspect Biol 2(3):a003350
19. Hayden MS, Ghosh S (2008) Shared principles in NF-kappaB signaling. Cell 132(3):344–362

20. Yu H et al (2020) Targeting NF-kappaB pathway for the therapy of diseases: mechanism and clinical study. Signal Transduct Target Ther 5(1):209
21. Luan B et al (2014) Leptin-mediated increases in catecholamine signaling reduce adipose tissue inflammation via activation of macrophage HDAC4. Cell Metab 19(6):1058–1065
22. Yang Q et al (2020) Histone deacetylase 4 inhibits NF-kappaB activation by facilitating IkappaBalpha sumoylation. J Mol Cell Biol 12(12):933–945
23. Asare Y et al (2020) Histone deacetylase 9 activates IKK to regulate atherosclerotic plaque vulnerability. Circ Res 127(6):811–823
24. Wallner M et al (2020) HDAC inhibition improves cardiopulmonary function in a feline model of diastolic dysfunction. Sci Transl Med 12(525):eaay7205
25. Yang X et al (2020) Transgenic inhibition of astroglial NF-kappaB restrains the neuroinflammatory and neurodegenerative outcomes of experimental mouse glaucoma. J Neuroinflammation 17(1):252
26. Lattke M et al (2017) Transient IKK2 activation in astrocytes initiates selective non-cell-autonomous neurodegeneration. Mol Neurodegener 12(1):16
27. Chen Y et al (2011) HDAC-mediated deacetylation of NF-kappaB is critical for Schwann cell myelination. Nat Neurosci 14(4):437–441
28. Leus NG, Zwinderman MR, Dekker FJ (2016) Histone deacetylase 3 (HDAC 3) as emerging drug target in NF-kappaB-mediated inflammation. Curr Opin Chem Biol 33:160–168
29. Zhang WB et al (2019) Inhibition of HDAC6 attenuates LPS-induced inflammation in macrophages by regulating oxidative stress and suppressing the TLR4-MAPK/NF-kappaB pathways. Biomed Pharmacother 117:109166
30. Xu C et al (2021) Histone deacetylase 5 deacetylates the phosphatase PP2A for positively regulating NF-kappaB signaling. J Biol Chem 297(6):101380
31. Li B et al (2021) HDAC5 promotes intestinal sepsis via the Ghrelin/E2F1/NF-kappaB axis. FASEB J 35(7):e21368
32. Lian H et al (2015) NFkappaB-activated astroglial release of complement C3 compromises neuronal morphology and function associated with Alzheimer's disease. Neuron 85(1):101–115
33. Litvinchuk A et al (2018) Complement C3aR inactivation attenuates tau pathology and reverses an immune network deregulated in tauopathy models and Alzheimer's disease. Neuron 100(6):1337-1353 e5
34. Shi Q et al (2017) Complement C3 deficiency protects against neurodegeneration in aged plaque-rich APP/PS1 mice. Sci Transl Med 9(392):eaaf6295
35. Hammond JW et al (2020) Complement-dependent synapse loss and microgliosis in a mouse model of multiple sclerosis. Brain Behav Immun 87:739–750